energies

MDPI

Article

Second-Order Sliding-Mode Control Applied to Microgrids: DC & AC Buck Converters Powering Constant Power Loads

Miguel Monsalve-Rueda [1], John E. Candelo-Becerra [2] and Fredy E. Hoyos [2,*]

[1] Facultad de Minas, Departamento de Procesos y Energía, Universidad Nacional de Colombia, Sede Medellín, Carrera 80 No. 65-223, Robledo, Medellín 050041, Colombia; memonsalver@unal.edu.co
[2] Facultad de Minas, Departamento de Energía Eléctrica y Automática, Universidad Nacional de Colombia, Sede Medellín, Carrera 80 No. 65-223, Robledo, Medellín 050041, Colombia; jecandelob@unal.edu.co
* Correspondence: fehoyosve@unal.edu.co; Tel.: +57-4-4309000

Abstract: Microgrids are designed to connect different types of AC and DC loads, which require robust power controllers to achieve an efficient power transfer. However, the effects of both AC and DC disturbances in the same type of controller make achieving stability a design challenge, especially in coupled systems where disturbances affect both the upstream and downstream in the microgrid. This paper presents an analysis of a second-order sliding-mode control (SOSMC) applied to a microgrid with direct-current (DC) and alternating-current (AC) power converters. The aim is to simulate the second-order sliding-mode control with buck converters that feed constant DC–DC and DC–AC power loads. The controller was tested in consideration of a unique sliding surface facing external disturbances, such as variations in the frequency of AC converters, sudden changes in upstream voltages, and constant power loads (CPL). The influence of the gain values (K) on the controller was also analyzed. The results show that the controller is robust regarding its sensitivity to external disturbances and steady-state error. However, the importance of the constant "K" in the model states that there exist K-limit values where if "K" is too low, a slowdown is presented, and the response against disturbances can be critical, and if is too high, an overshoot is presented in the output voltage.

Keywords: sliding-mode control; microgrid; buck converter; constant power load; power converter

check for updates

Citation: Monsalve-Rueda, M.; Candelo-Becerra, J.E.; Hoyos, F.E. Second-Order Sliding-Mode Control Applied to Microgrids: DC & AC Buck Converters Powering Constant Power Loads. *Energies* **2024**, *17*, 2701. https://doi.org/10.3390/en17112701

Academic Editors: Sreedhar Madichetty and Abdelkader El Kamel

Received: 12 April 2024
Revised: 20 May 2024
Accepted: 30 May 2024
Published: 2 June 2024

Copyright: © 2024 by the authors. Licensee MDPI, Basel, Switzerland. This article is an open access article distributed under the terms and conditions of the Creative Commons Attribution (CC BY) license (https://creativecommons.org/licenses/by/4.0/).

1. Introduction

A microgrid (MG) is continuously subject to disturbances and uncertainties due to the natural variability in power supplies and loads [1]. MGs require robust controls, and the second-order sliding-mode control (SOSMC) has been demonstrated to be robust in a wide range of applications: photovoltaic energy conversion [2], medical, aerospace, power converters [3–5], and others [6]. It is crucial to continue with the study as the environmental and energy challenges of society suggest that they contribute to the sustainability and reliability of electrical networks [7,8]. Consequently, investigating how to improve the performance of MGs by designing a SOSMC is a very practical challenge.

SOSMC retains the advantages of the conventional sliding-mode control (SMC), such as reduced order dynamics, robustness, and stability. However, the main control objective in the multiple stages of an MG is to maintain the stability of the system, especially if the MGs have different types of loads, i.e., direct current (DC) and alternating current (AC), and different types of power sources (renewables and storage systems) sharing a common DC bus [8–11]. Then, the design and implementation of a SOSMC are required to address chattering effects [12–14] and increase reliability in an MG.

Robust control systems designed for MGs have implemented higher-order SMC to alleviate chattering [15], which is one of the most significant drawbacks of conventional SMC [16,17]. Since a power converter is an essential element within an MG, these elements must be designed for multiple types of loads (i.e., DC/DC, DC/AC) to satisfy all the power

requirements of applications in the industry and residential grids [18,19]. Therefore, the control of MGs with different loads must be able to deal with uncertainties and disturbances [20]. The complexity of these systems, as they have so many diverse behaviors in their elements, means they require sufficiently robust control so that the loads are not affected by these disturbances. Moreover, stability is crucial if there is a cascade of power converters feeding constant power loads (CPL).

The authors in [5] proposed a suboptimal second-order controller that can work in grid-connected and island-connected operation modes, and the results are compared with the traditional PI control. The authors of [21] designed a super-twisted algorithm for DC–DC power converters. In [22], the author proposed two main criteria based on Lyapunov linearization and mixed potential theory to analyze the stability of the cascade system that feeds CPLs. In this research, our objective is to explore all previous concepts acting simultaneously: the use of a higher-order sliding-mode control with various power converters (DC–DC & DC–AC) and analyzing the stability of the system from a practical perspective. However, although these controllers offer novel solutions in terms of sliding control types, in none of these applications is a single control design tested simultaneously with different real-time applications. In this sense, the present investigation seeks to test the robustness of the control design against disturbances in various types of microgrid applications simultaneously, using a single set of second-order slider controller design parameters.

SMC is not a recent control technique that offers robustness; it is a particular case of what were initially called variable structure systems [23]. Several second-order controllers have been individually documented with buck converters [3,4,24,25]. In addition, [5,26] tested a suboptimal SOSMC with some variations, such as adaptive sliding control [27,28]. However, the actual performance of a SOSMC in an MG with multiple inverters for different types of load in AC and DC currents has not yet been tested. Thus, a very common MG must contain several stages in which different currents can feed other loads. However, more research is needed on multistage controls with different types of MG converters with AC and DC circuits testing a unique controller for all stages.

Therefore, this paper presents the design and implementation of a SOSMC in a hybrid (DC & AC loads) MG [9–11,29,30]. The system is proposed to examine the stability of an MG under certain typical disturbances (variations in loads, instability in sources, and alterations in voltage buses) [31,32]. Then, the MG considers CPLs [33–35] to observe the stability against disturbances. First, a microgrid model was implemented in MATLAB Simulink to emulate a real circuit with different sources and loads. In addition, the contributions in this paper are as follows:

1. SOSMC offers a fast and stable response to disturbances for AC and DC buses.
2. A single SOSMC can provide robustness to a microgrid that experiences disturbances in three stages (the Main Bus and A.C. and D.C. Buses), given that the appropriate manifold and parameters are selected.
3. The selection of the constant value in the SOSMC manifold is of utmost importance, as an improper choice of this value may lead to chattering and/or the overshoot phenomena in the output signal.

The paper contains three more sections. Section 2 presents the materials and methods used in this research, with mathematical fundamentals and simulations. Section 3 presents the results, analysis, and discussions obtained from the experiments. Finally, Section 4 considers the conclusions.

2. Materials and Methods

2.1. General Methodology

The methodology used a dynamic model representing a circuit as an object of study attached to a microgrid. The model was created in Simulink using the SimScape library to emulate real applications and disturbances.

Previous studies indicate that the control is robust in a microgrid as long as other strategies, such as adaptive control, are used simultaneously: in [27], the paper presents an

adaptive suboptimal second-order controller that can work in grid-connected and island operation modes, and the results are compared with traditional PI control. In [21], the paper presents a super-twisted algorithm for DC–DC power converters. In [22], the author proposes two main criteria based on Lyapunov linearization and a mixed potential theory to analyze the stability of cascade system feeding CPLs, similarly to [36]. In other applications such as robotics, this type of adaptive sliding control is also used as in [37,38]. Another technique such as fuzzy logic controller based on sliding-mode control is also proposed in [39]. Similarly, in a previous work, we compared the response between a PID control versus an SMC control in a buck converter with CPL [40]. In this research, we aim to explore some previous concepts acting simultaneously: using a higher-order sliding-mode control with diverse power converters (DC–DC & DC–AC) and analyzing the system stability from a practical perspective, simulating a real application of a microgrid. The innovation is that this type of work, where a single controller is evaluated and analyzed in all stages of a complete microgrid, is scarce in the current literature.

The implemented system is a three-stage microgrid. The first stage is a main bus with the control objective of maintaining stability in the DC bus against possible disturbances. The second stage is a circuit with a DC/AC controller aiming to guarantee waveform and frequency stability in the face of sudden changes upstream and in the loads. The final stage is a circuit with its controller for DC loads. All controllers consider a second-order sliding-mode control and share a single parameter layout. In this sense, it is considered a system with a single design that has not been previously tested in the current literature.

2.2. Architecture

The microgrid is a small and smart power system with power sources, AC buses, DC buses, power controllers, and loads. Figure 1 shows the DC–AC microgrid implemented that includes the basic elements to supply the power demand.

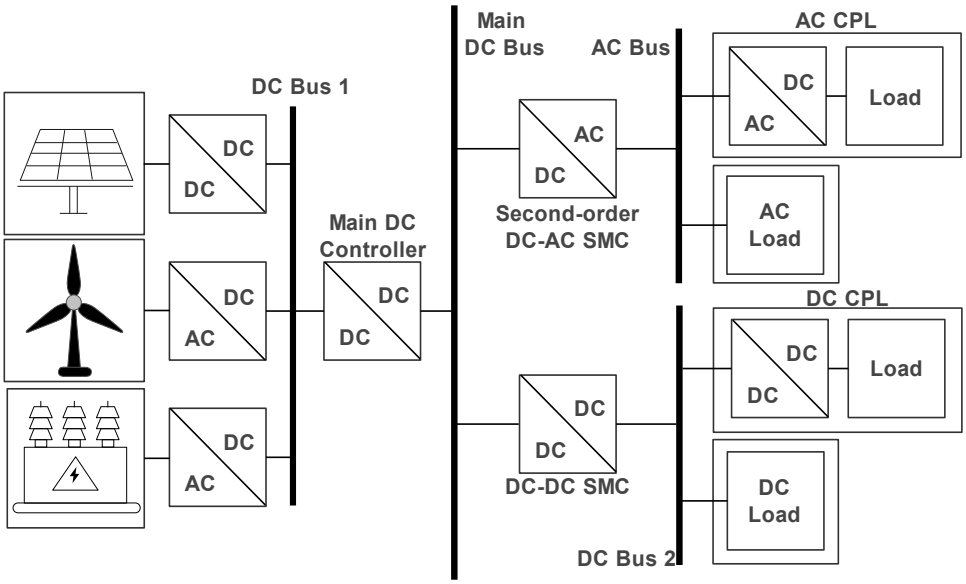


Figure 1. Diagram of the AC–DC microgrid.

On the left side of Figure 1, the microgrid considers renewable energies such as photovoltaic and wind generators, and an AC power grid is also connected. All these sources have power converters to transfer power from DC or AC circuits to the DC Bus 1. Then, in the first Main DC controller, a SOSMC is implemented to control the Main DC Bus, which regulates the voltage at this point. After the main DC controller, two additional controllers are dedicated to keeping the voltage stable in the loads. The second controller is a DC–DC SOSMC that regulates the voltage to a DC CPL load. The third controller is a DC–AC SOSMC that regulates the voltage on the AC Bus where an AC CPL is connected.

These three controllers mentioned previously are the objects of analysis, mainly. For the Main DC Controller and DC–DC SMC, the circuit uses DC–DC buck converters with the following parameters defined in Table 1.

Table 1. Parameters for the DC–DC buck converter.

Item	Element	Value
1	Load Resistor	10 Ω
2	Inductance	2.47 mH
3	Capacitor	46 µF
4	Source	320 V
5	Vreference	120 VRMS
6	Frequency	60 Hz
7	Disturbance Resistor	2 Ω

2.3. Power Controller

Figure 2 presents the diagram of the AC and DC loads connected to the microgrid and Figure 3 shows the diagram of the circuit implemented in Matlab/Simulink version 2018a. The Main DC Bus voltage is obtained by controlling a DC–DC buck converter. The DC Bus 2 voltage is the result of the response of the second controller, aiming at a set point established as required by the application. For the AC Bus, a third SOSMC controller was implemented; the full-bridge inverter is a typical inverter that requires four switches simultaneously, as presented in Figure 2, which are controlled by u_3 and $\bar{u}_3$ control signals. Finally, the AC CPL and the DC CPL were also designed using buck converters controlled by SOSMC. In this model, the switch used was the MOSFET. The design of the parameters for the previous buck converters was calculated depending on the typical operational conditions of each stage. The red and blue colors in Figure 2 refer to direct current voltage polarities.

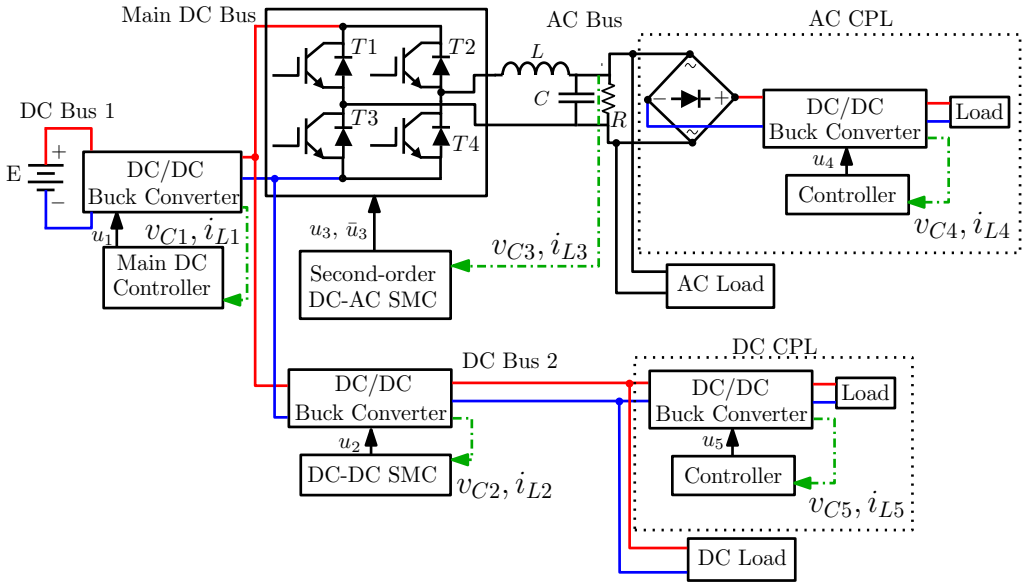


Figure 2. Diagram of the AC and DC loads connected to the microgrid.

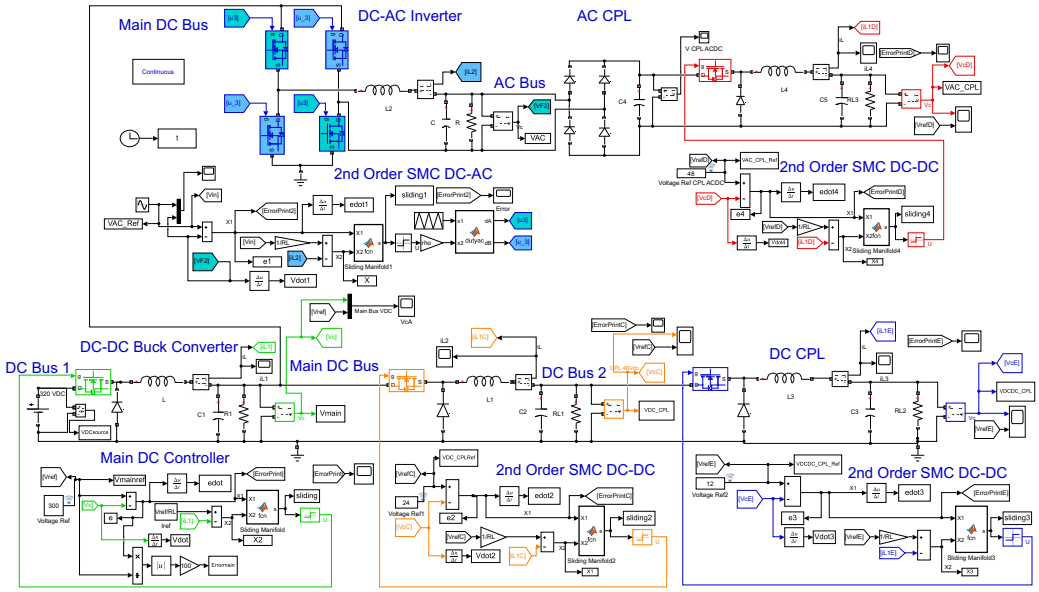


Figure 3. Diagram of the circuit implemented in MATLAB-Simulink.

2.4. Mathematical Model of the Controller

Figure 4 presents the circuit model of the buck converter connected to a CIL and a CPL. The total current supplied by the electrical circuit is equal to the sum of the current in the CIL, and the current in the CPL is as shown in Equation (1):

$$i_{bus} = \frac{v_c}{R} + \frac{P}{v_c} \tag{1}$$

where i_{bus} is the current supplied by the circuit, R is the constant resistance of the CIL, P is the active power of the CPL, and v_c is the voltage of the capacitor. The equivalent resistance of the circuit can be obtained according to the voltage and the current in the bus, as expressed in Equation (2):

$$R_{eq} = \frac{v_c}{i_{bus}} \tag{2}$$

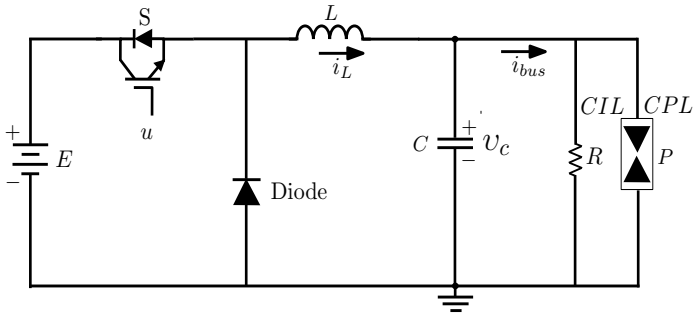


Figure 4. Circuit model of the buck connected to the CIL (R) and CPL (P).

2.5. Dynamics of Buck Converter (PC SMC)

The mathematical models used to represent the dynamics of a buck converter that feeds the CIL and the CPL are presented in Equations (3) and (4):

$$L\frac{di_L}{dt} = uE - v_c \tag{3}$$

$$C\frac{dv_c}{dt} = i_L - \frac{v_c}{R} - \frac{P}{v_c} \tag{4}$$

In these equations, the term L is the inductor, C is the capacitor, v_c is the instantaneous voltage of the capacitor, and i_L is the instantaneous current of the inductor. As defined previously in the model, the term E is the voltage of the power source. The term R represents the constant resistance of the load connected to the bus, P is the active power of the load, and the term u is used to represent the switching function with values $\{0,1\}$.

2.6. Response of Controller

Robust control systems designed for microgrids have implemented higher-order sliding-mode control to alleviate chattering, one of the most significant drawbacks of conventional sliding control. Since a power converter is an essential element within a microgrid, these elements must be designed for multiple types of loads (i.e., DC/DC and DC/AC) to satisfy all the power requirements of the applications in industrial and residential grids. Therefore, control of microgrids with different loads must be able to deal with uncertainties and disturbances. The complexity of these systems, as they have so many diverse behaviors in their elements, means they require sufficiently robust control so that the loads are not affected by these disturbances. In addition, stability is crucial if there is a cascade of power converters that feed the CPLs.

SOSMC keeps the main properties and is a generalization idea of first-order SMC. However, from a geometric standpoint, in SOSMC, the sliding surface is the line after the intersection of the two perpendicular planes $\sigma = 0$ and $\dot{\sigma} = 0$, and the states will approach the equilibrium point through this trajectory, as presented in Figure 5.

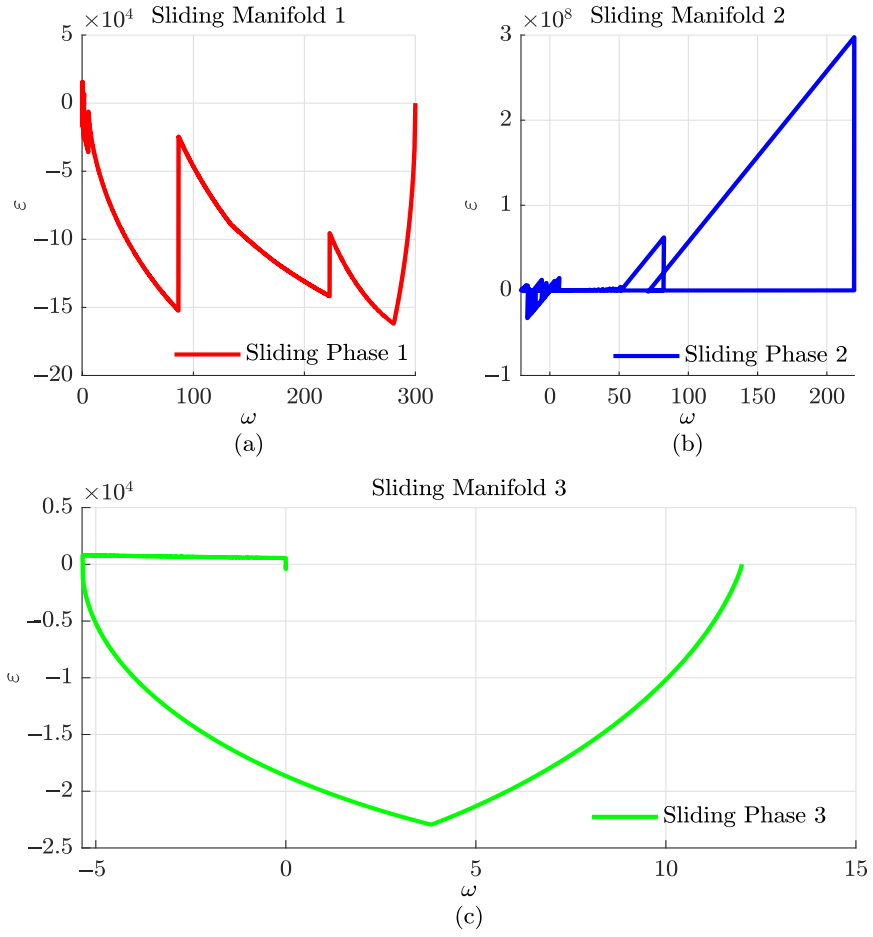


Figure 5. Phase portraits for the three controllers in the MG.

Figure 5 shows the phase portrait for the main controller. This figure shows the phase diagrams for the three controllers. Manifold 1 corresponds to the main DC controller,

Manifold 2 to the DC–AC controller, and Manifold 3 to the DC–DC Controller. Those phase diagrams illustrate how a second-order sliding control goes toward the origin in finite time. This is one of the fundamental properties of sliding control.

The control objective states require that $\sigma \overset{yields}{\longrightarrow} 0$ and $\dot{\sigma} \overset{yields}{\longrightarrow} 0$. Then, in general, we choose the sliding surface:

$$\sigma = X_2 + cX_1 \tag{5}$$

where:

$$X_1 = v_{cref} - v_c \tag{6}$$

$$X_2 = i_{ref} - i_L \tag{7}$$

So, if we consider the next sliding variable,

$$\sigma = X_2 + c|X_1|^{1/2}.sign(X_1) \tag{8}$$

Then, the new manifold will be

$$X_2 + c|X_1|^{1/2}.sign(X_1) = 0 \tag{9}$$

Here, X_1 and X_2 in a buck converter are the errors in voltage and current, respectively. In such a way, the controller

$$u = -\rho sign(\sigma) \tag{10}$$

Then, replacing from Equation (9), we obtain

$$u = -\rho sign(X_2 + c|X_1|^{1/2}.sign(X_1)) \tag{11}$$

With

$$\rho >> 0$$

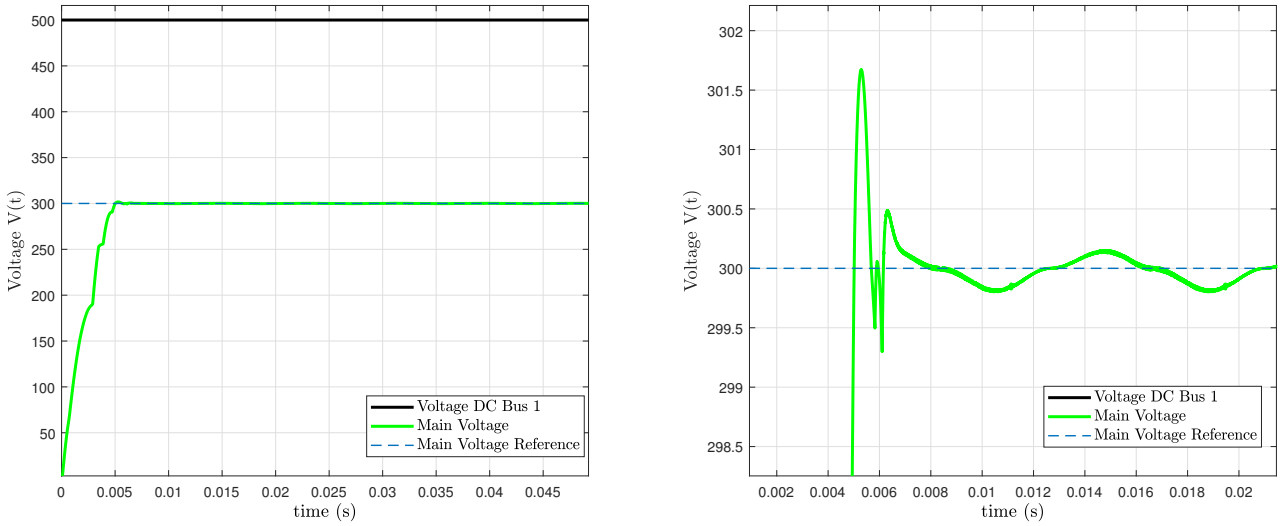
As stated by the author of [41], one of the main particularities in this control is that the SOSMC derivative acts on the sliding variable instead of affecting the first-order derivative. This is performed to push the sliding variable to zero in a finite time and is one way to prove that functions with the same characteristics of u maintain stability in more general spaces (i.e., Banach) [42,43].

3. Results and Analysis

This section presents the results and analysis of the SOSMC's application to the buck converter and its behavior after disturbances. The results aim to show the effectiveness of the SOSMC in the microgrid. Disturbances were considered to be changes in the voltage reference of the main DC bus, voltage of DC Bus 1, AC frequency (from 60 to 120 Hz), and voltage of the CPL.

3.1. SOSMC in a DC–AC Buck Converter

Figure 6a shows the response of the buck converter when the reference voltage is set up to 300 Vdc. In this case, the voltage of the DC 1 bus is 400 Vdc. Figure 6b presents a zoom of the initial response to observe the overshoot and settling time. The result indicates that the maximum positive overshoot is 301.75 Vdc, corresponding to 0.71%. The maximum negative overshoot is 299.4 Vdc, corresponding to 0.83%. The settling time for a 2% band is 14 ms. After this event, the system reaches the steady-state stability given by the reference value.



(**a**) (**b**)

Figure 6. Behavior of the buck converter controlled by SOSMC: (**a**) response to a 300 Vdc step and (**b**) zoom to see overshoot and settling time.

3.2. Variations in Voltage Reference of the Main DC Bus

Figure 7 presents the response of the circuit to a main disturbance in the main DC bus. All plots are graphed in the time domain from 0 to 0.15 s. Figure 7a represents the main DC controller response with changes at the set point. Initially, the reference signal was changed from 0 to 300 Vdc at 0 s. Then, a change from 300 to 400 Vdc was made at 20 ms. Subsequently, a change from 400 to 450 Vdc was made at 40 ms. Then, a change was made from 450 to 400 Vdc. Finally, a change was made from 300 to 100 Vdc.

The results in Figure 7a show that when the first reference is changed to 300 Vdc, an overshoot is presented, and it is greater than the other overshoots. Reference signals less than 155 Vdc are excluded from this rule, which corresponds to the peak value of the AC bus because this bus requires that it be maintained at 110 Vrms, which corresponds to the 155 Vac peak value. Furthermore, as this bus is downstream, the main bus signal cannot be less than this value because the controller cannot maintain the AC bus voltage. It is also observed that the settling time for decreasing references is longer because the buck converter used to control the main bus uses only one MOSFET. Therefore, the main DC voltage keeps its control value once in the stable region.

Figure 7b presents the behavior of the AC voltage in the CPL, which does not present significant variations in the signals after disturbances. Figure 7c presents the voltage behavior in the DC–AC CPL for a reference of 48 Vdc, showing that the controller responds quickly to changes and stabilizes the signal. Figure 7d shows the voltage in the DC bus when the voltage reference is set to 24 Vdc; it indicates that the voltage stabilizes quickly at the value established for the reference. Figure 7e shows the voltage on the CPL bus for a 12Vdc reference, showing that the signal remains stable after the first change and presenting a first overshoot that is quickly stabilized. Therefore, these last four figures show that with the SOSMC controls, the voltages stabilize after the disturbance. In addition, it can be observed that it regulates the DC signals, and these do not affect the signals of the upstream and downstream buses. Finally, despite the strong upstream variations, the DC bus and its load (DC voltage in the CPL) remain at their set points.

Table 2 summarizes the results presented in the previous figures. The first column corresponds to the time in seconds. The second column is the response on the main DC bus. The third column is the response of the AC bus. Finally, the fourth column corresponds to the response in the CPL.

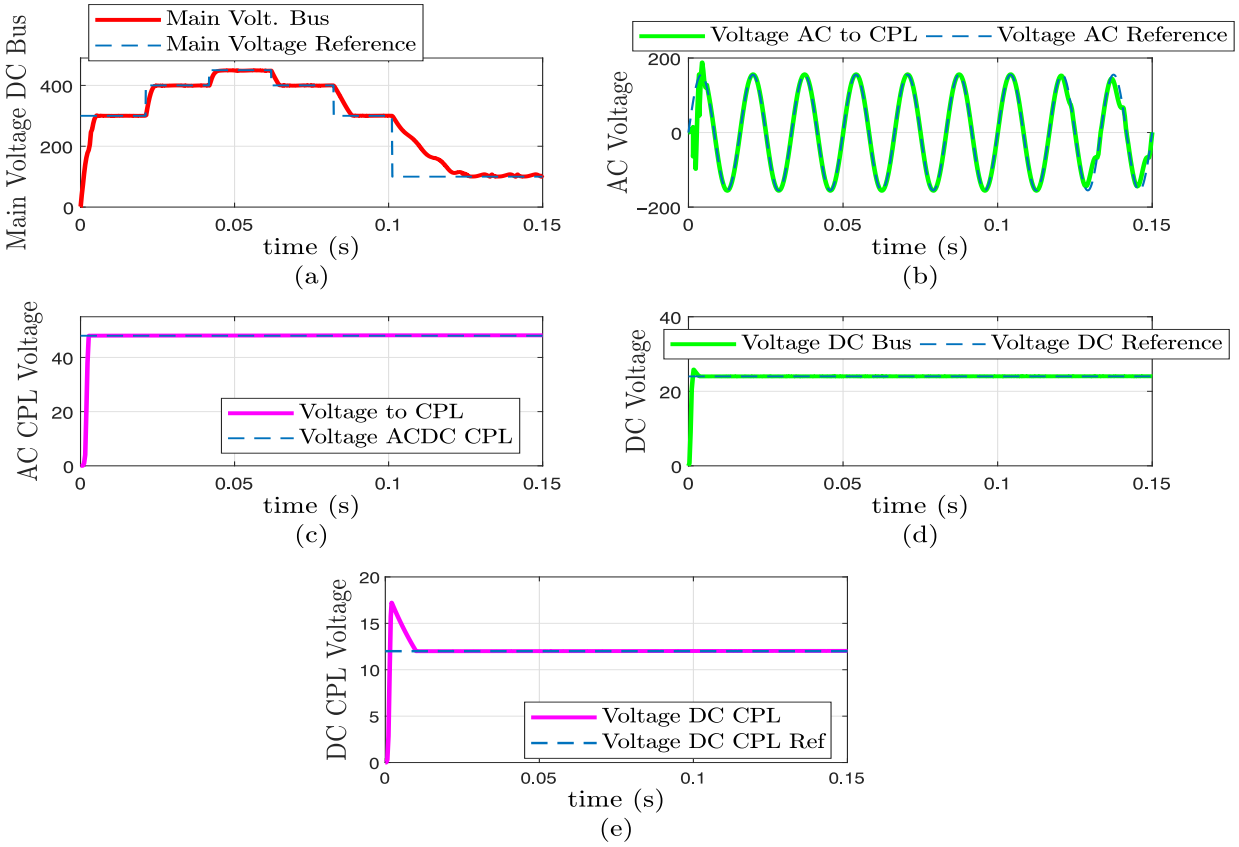


Figure 7. Behavior of voltages after a disturbance in the main DC bus: (**a**) main DC bus, (**b**) AC bus, (**c**) AC CPL, (**d**) DC Bus 2, and (**e**) DC CPL.

Table 2. Time analysis after a disturbance on the main DC bus.

Time (s)	Main DC Bus	AC Bus	CPL
0–0.02	Initial response, reaching a set point of 300 Vdc. Settling time: 0.14 ms. Overshoot: 1.33%.	AC signal stable after 7 ms	AC CPL reaches the reference after 7 ms, and DC CPL reaches the reference after 7 ms
0.02–0.04	Reaching a set point of 400 Vdc. Settling time: 0.12 ms. Overshoot: 5.53%.	AC signal stable	Both CPLs keep stable
0.04–0.06	Reaching a set point of 450 Vdc. Settling time: 6 ms. Overshoot: 5.53%.	AC signal stable	Both CPLs keep stable
0.06–0.08	Down to a set point of 400 Vdc. Settling time: 6 ms. Overshoot: 5.53%.	AC signal stable	Both CPLs keep stable
0.08–0.1	Down to a set point of 300 Vdc. Settling time: 6 ms. Overshoot: 5.53%.	AC signal stable	Both CPLs keep stable
0.1–0.14	Down to a set point of 100 Vdc. Settling time: 6 ms. Overshoot: 5.53%.	AC signal unstable after 0.12 s	Both CPLs keep stable

3.3. Voltage Reference Changes in DC Bus 1

Figure 8 presents the voltage behavior in the main DC bus after a disturbance in DC Bus 1. A change in the voltage of DC Bus 1 is made from 500 Vdc to 400 Vdc at 0.05 s. Then,

a change is made from 400 Vdc to 500 Vdc at 0.1 s. It is observed that the voltage on the main DC bus remains stable, and no changes are observed due to disturbances. The behavior of the transient before 20 ms is normal, as shown in the previous analysis.

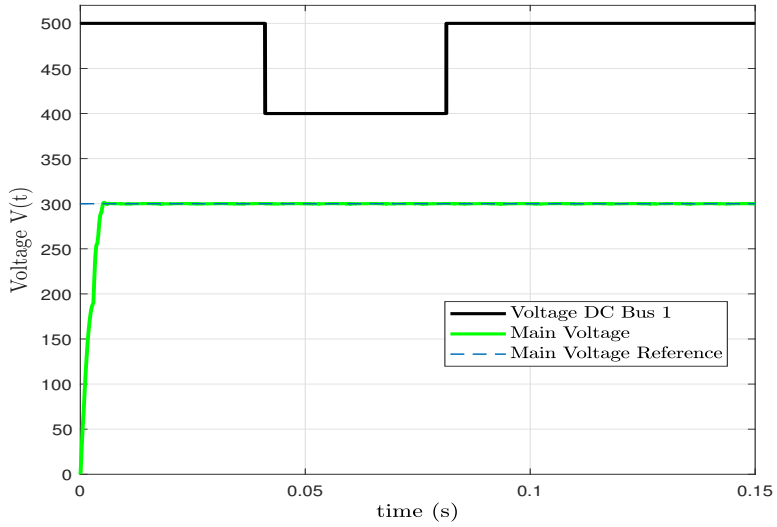
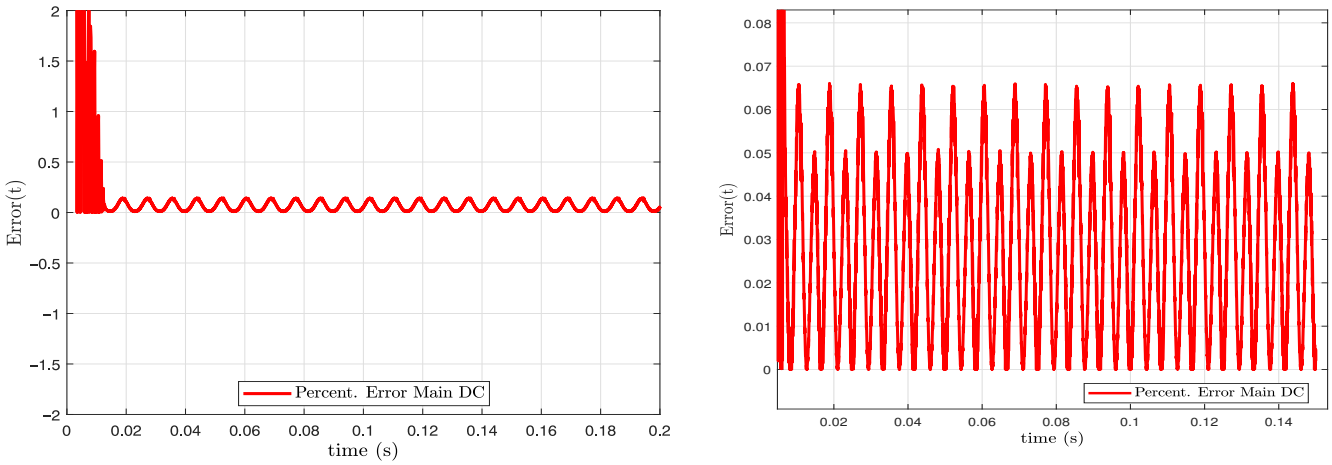


Figure 8. Voltage of the main DC bus after a disturbance in DC Bus 1.

Figure 9 presents the error of the SOSMC. Figure 9a shows the percentage error on the main DC bus, and Figure 9b presents a zoom of the percentage error from 10 to 50 ms. In the first 10ms, the error is large because of the reference change; however, this result presents normal behavior. After this first time, the results show a small error of 0.065%.



(**a**) (**b**)

Figure 9. Sliding-mode controller error: (**a**) percentage error on the main DC bus and (**b**) zoom of the percentage error on the main controller.

Figure 10 presents the behavior of the voltage in the main DC bus regarding the variation of the parameter k. Figure 10a shows the voltage when the parameter $k = 0.5$, Figure 10b shows the voltage when the parameter $k = 3$, Figure 10c shows the voltage when the parameter $k = 10$, Figure 10d shows the voltage when the parameter $k = 15$, Figure 10e shows the voltage when the parameter $k = 20$, and Figure 10f shows the voltage when the parameter $k = 80$.

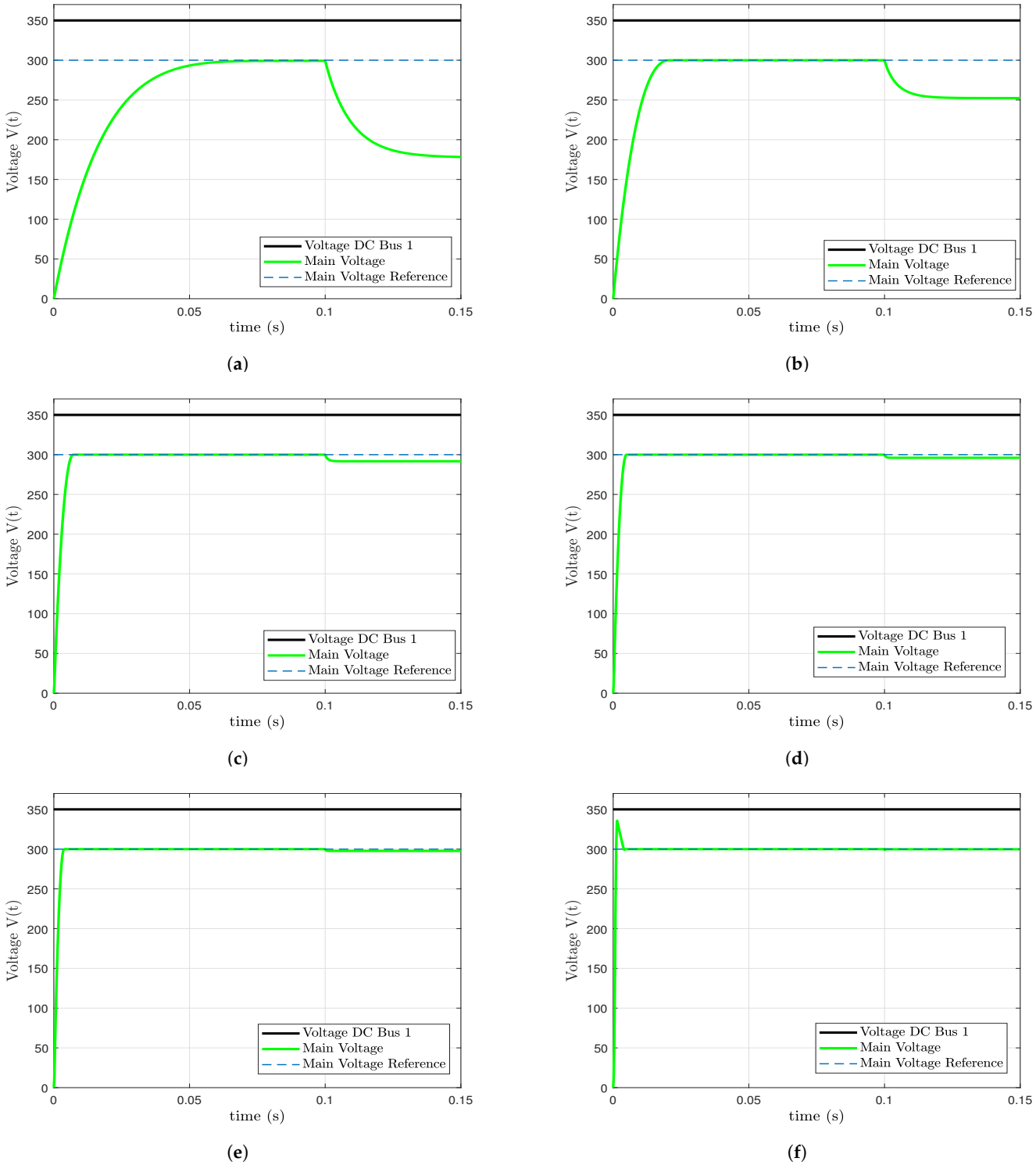


Figure 10. Voltages with respect to variation in parameter k: (**a**) $k = 0.5$, (**b**) $k = 3$, (**c**) $k = 10$, (**d**) $k = 15$, (**e**) $k = 20$, and (**f**) $k = 80$.

Figure 11 presents the controller response after the voltage reference in the main bus was abruptly disturbed from 250 Vdc to 320 Vdc. Furthermore, Figure 12 presents the settling time after the change is made from 320 Vdc to 230 Vdc.

The result shows that the output signal follows the reference signals. These results demonstrate that the DC bus and CPL voltages are stable, despite this intense variation. Furthermore, the results in Figures 11 and 12 show that the time to reach a new voltage

reference is shorter than that required for a lower voltage reference. This is due to the very nature of the converter, as it acts only on MOSFET devices, and its response to decreasing the voltage depends on internal elements such as capacitors and coils.

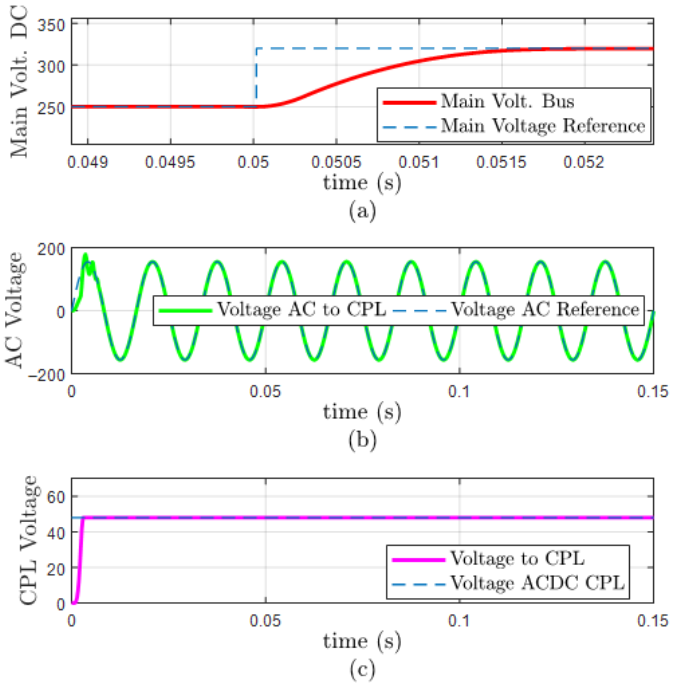


Figure 11. Settling time after an up variation in the set point: (**a**) main voltage, (**b**) AC voltage, and (**c**) CPL voltage.

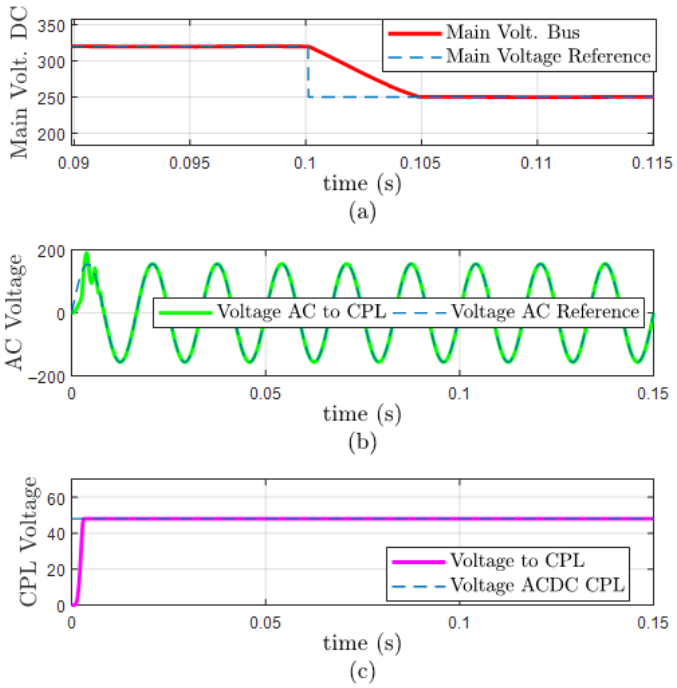


Figure 12. Settling time after a down variation in the set point: (**a**) main voltage, (**b**) AC voltage, and (**c**) CPL voltage.

3.4. Change in the Voltage of DC Bus 1

In a microgrid, commonly, the main voltages fluctuate depending on the sources (i.e., cloud interference on a PV array and wind intermittence on a wind power turbine). Therefore, the following simulations perform some disturbances to evaluate the controller response in the microgrid.

Figure 13 presents the behavior of the voltage in the main bus after a variation in the DC bus from 250 to 320 Vdc ($t = 0.05$ s). Then, when $t = 0.1$ s, a new variation is considered, from 320 to 220 Vdc. This figure presents three plots: Figure 13a is related to the main voltage bus, Figure 13b shows the DC voltage, and Figure 13c shows the AC–DC CPL voltage. All plots are graphed in the time domain from 0 to 0.15 s. This result establishes that the SOSMC controls maintain all the set points stably after a strong disturbance.

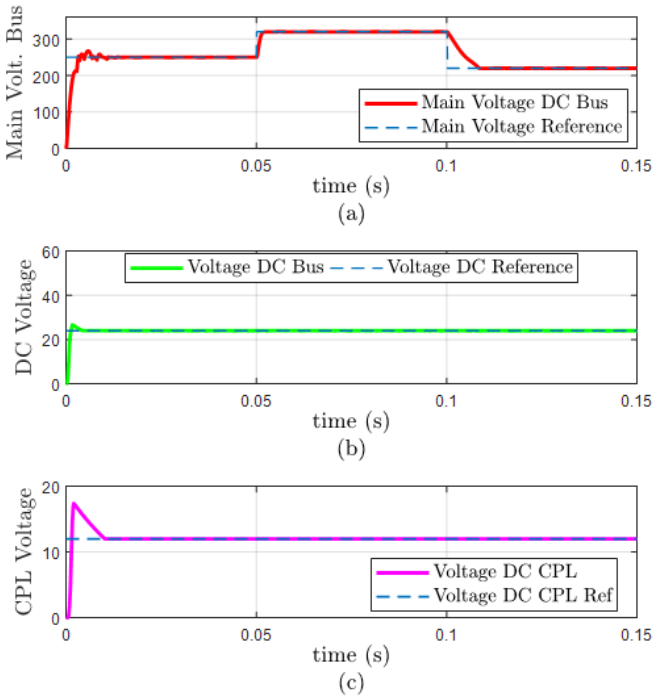


Figure 13. Behavior of voltages when the reference changes in the DC bus: (**a**) main bus, (**b**) DC bus, and (**c**) CPL bus.

3.5. Frequency Reference Variation in the AC Bus

Figure 14 shows the results after a disturbance in the system, given by the change in the frequency of the AC bus. Figure 14b presents the variation in the frequency of the AC bus from 60 Hz to 120 Hz ($t = 0.05$ s) VAC and then vice versa ($t = 0.1$ s), simulating a disturbance. This figure presents five plots: Figure 14a shows the voltage diagram related to the main voltage bus, Figure 14b is the frequency perturbation for the AC bus, Figure 14c shows the voltage of the DC bus, Figure 14d shows the voltage of the DC–DC CPL, and Figure 14e presents the voltage of the DC–AC CPL. All plots are graphed in the time domain from 0 to 0.15 s. This result demonstrates that, despite a powerful disturbance in frequency, the branch in DC voltages remains stable.

Figure 15 shows the voltages of the system in the main DC bus, AC bus, and DC Bus 2 after a disturbance on the AC CPL. The perturbation was applied in Figure 15d. Figure 15a indicates that the main DC bus remains stable after the perturbation on the AC CPL. The same behavior is observed for the DC branch with the DC CPL in Figures 15c,e. All plots are graphed in the time domain from 0 to 0.15 s.

This result demonstrates that, despite a strong disturbance in the AC CPL branch, the main DC voltage and the secondary bus remain immovable.

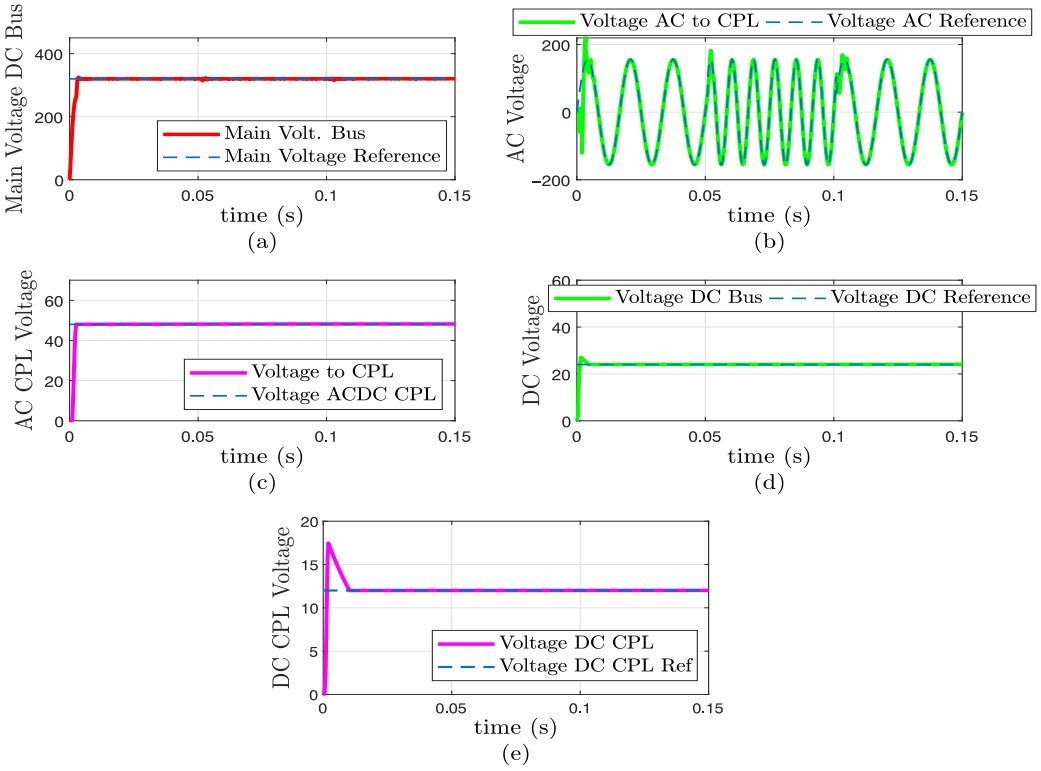


Figure 14. Behavior of voltages with a frequency change from 60 to 120 Hz. (**a**) Main DC bus, (**b**) AC bus, (**c**) AC CPL, (**d**) DC Bus 2, and (**e**) DC CPL.

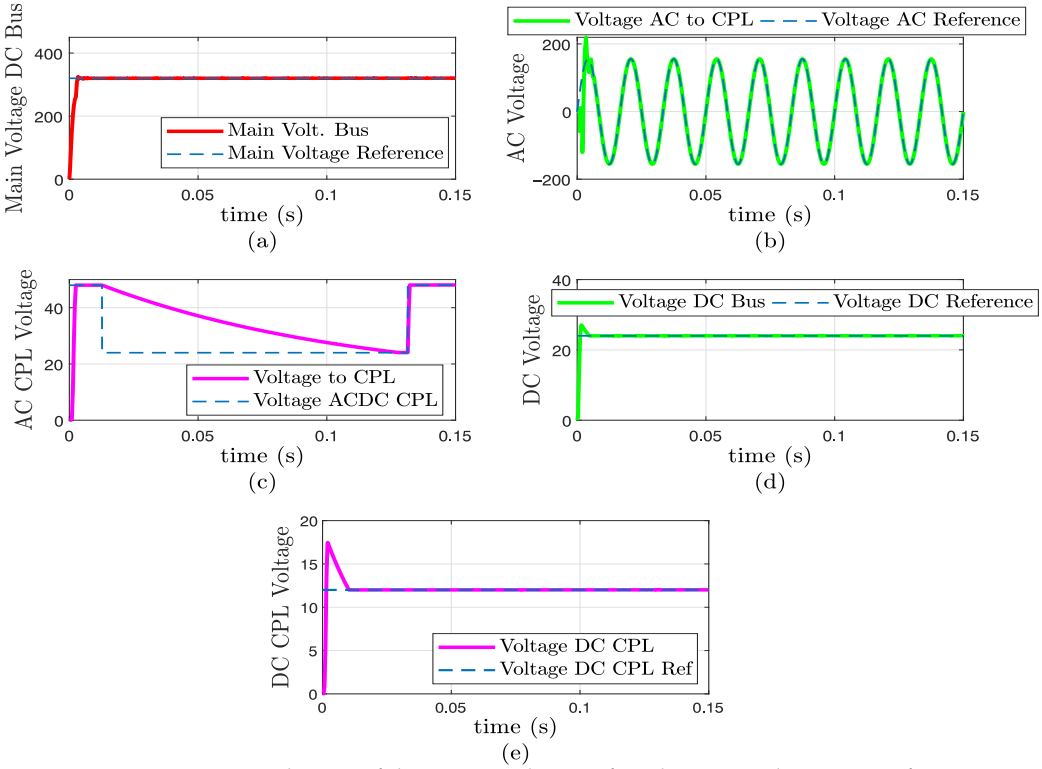


Figure 15. Behavior of the circuit voltages after changes in the set point from 48 to 24 Vdc and from 24 to 48 Vdc. (**a**) Main voltage DC bus, (**b**) AC voltage, (**c**) AC CPL voltage, (**d**) DC voltage, and (**e**) DC CPL voltage.

Figure 16a,b show the results after a disturbance in the system caused by a change in the voltage of the AC–DC CPL. Figure 16a presents the AC–DC branch after a variation in the AC–DC CPL from 12 Vdc to 18 Vdc ($t = 0.05$ s) and then vice versa ($t = 0.1$ s), simulating a disturbance. This figure presents three plots: Figure 16a shows the voltage behavior related to the main voltage bus, Figure 16b shows the voltage behavior of the DC voltage bus, and Figure 16c shows the voltage behavior of the DC–DC CPL voltage. All plots are graphed in the time domain from 0 to 0.15 s.

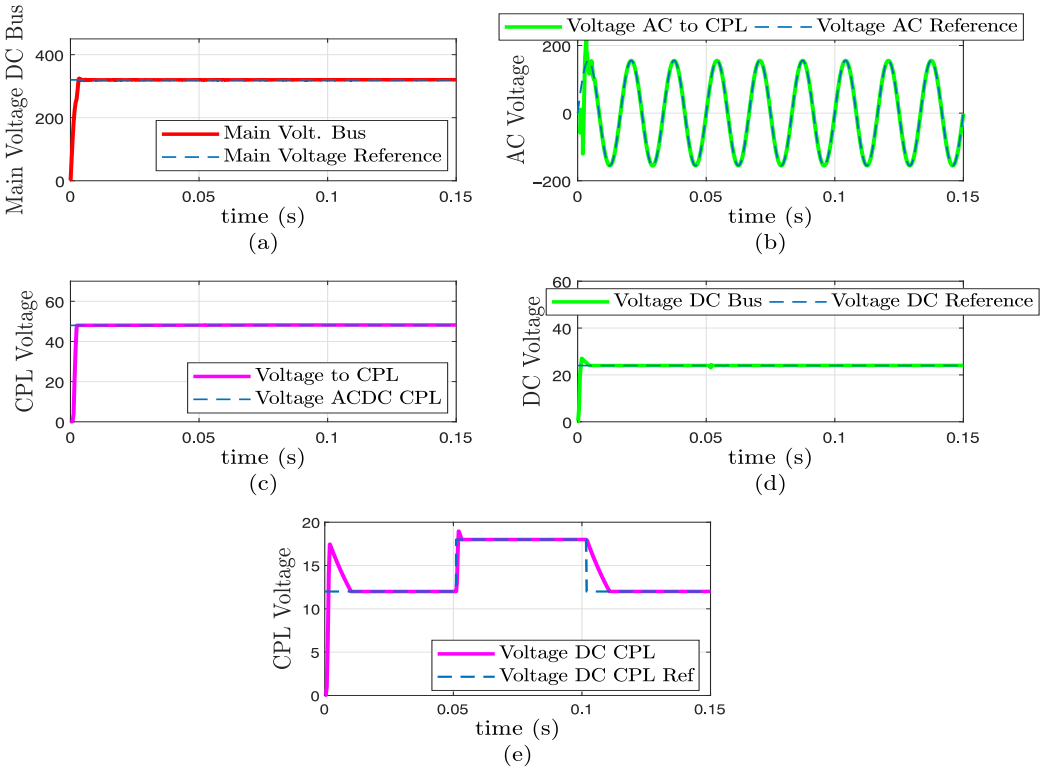


Figure 16. Voltage behavior after a change in voltage reference in the DC–DC CPL from 12 to 18 Vdc: (**a**) main bus, (**b**) AC bus, (**c**) CPL bus, (**d**) DC voltage, and (**e**) DC CPL voltage.

4. Conclusions

This paper presented the design of a SOSMC to operate in a DC–AC microgrid. The results allow us to infer the following conclusions:

- The SOSMC demonstrated robustness in the microgrid, with a stable response in terms of voltage and frequency for commercial applications. The average error during the simulations was less than 0.2% for disturbances of 28% in the main voltage feeder.
- The constant on the design surface, which must be >0, represents substantial consequences in the controller response. The correlation showed that a higher value of k produces a faster response. However, it will be overcome with a higher chattering effect at a determined value (greater than 25 for this particular application). Furthermore, a higher value of k will have a higher capacity to compensate for disturbances.
- SMC is not a novel control. However, the demonstrations presented in this work show evidence that, for modern applications, it is considered to have robust behavior. With a simple mathematical model, applied from a practical standpoint in an application of high relevance and importance, it was shown to provide the required stability for industrial and residential microgrid applications.
- In the case of alternating-current controllers, it was observed that the second-order controller presents outstanding stability, even for changes in the frequency of up to 60 Hz concerning its original set point. The SOSMC demonstrated stable performance

against frequency variations: after a substantial variation of 60 Hz (from 60 to 120 Hz) in the input signal set point, the SOSMC maintained stability in all stages of the MG.
- In DC–DC converters, simple and SOSMC controllers showed a much higher response speed and less overshoot than the conventional PID-type control.
- There are still restrictions from the methodological standpoint, such as the dependence on the sampling frequency, since different results are obtained depending on the selection of this frequency value. It is suggested to continue the investigation into a completely real model with real microgrid loads that allows for the validation of the findings. In this way, the functionality of the SMC controllers would be empirically demonstrated.

Author Contributions: Conceptualization, investigation, methodology, and software, M.M.-R. Formal analysis, writing—review, and editing, M.M.-R., J.E.C.-B. and F.E.H. All authors have read and agreed to the published version of the manuscript.

Funding: This work was supported by the Universidad Nacional de Colombia Sede Medellín under the project HERMES-61430.

Data Availability Statement: The original contributions presented in the study are included in the article, further inquiries can be directed to the corresponding author.

Acknowledgments: The work of Fredy E. Hoyos and John E. Candelo-Becerra was supported by the Universidad Nacional de Colombia, Sede Medellín.

Conflicts of Interest: The authors declare no conflict of interest.

References

1. Ahmad, S.; Shafiullah, M.; Ahmed, C.B.; Alowaifeer, M. A Review of Microgrid Energy Management and Control Strategies. *IEEE Access* **2023**, *11*, 21729–21757. [CrossRef]
2. Gursoy, M.; Zhuo, G.; Lozowski, A.G.; Wang, X. Photovoltaic Energy Conversion Systems with Sliding Mode Control. *Energies* **2021**, *14*, 6071. [CrossRef]
3. Ding, S.; Zheng, W.X.; Sun, J.; Wang, J. Second-Order Sliding-Mode Controller Design and Its Implementation for Buck Converters. *IEEE Trans. Ind. Inf.* **2018**, *14*, 1990–2000. [CrossRef]
4. RakhtAla, S.M.; Yasoubi, M.; HosseinNia, H. Design of second order sliding mode and sliding mode algorithms: A practical insight to DC-DC buck converter. *IEEE/CAA J. Autom. Sin.* **2017**, *4*, 483–497. [CrossRef]
5. Cucuzzella, M.; Incremona, G.P.; Ferrara, A. Design of Robust Higher Order Sliding Mode Control for Microgrids. *IEEE J. Emerg. Sel. Top. Circuits Syst.* **2015**, *5*, 393–401. [CrossRef]
6. Le Nhu Ngoc Thanh, H.; Hong, S.K. Quadcopter Robust Adaptive Second Order Sliding Mode Control Based on PID Sliding Surface. *IEEE Access* **2018**, *6*, 66850–66860. [CrossRef]
7. Khan, M.R.; Haider, Z.M.; Malik, F.H.; Almasoudi, F.M.; Alatawi, K.S.S.; Bhutta, M.S. A Comprehensive Review of Microgrid Energy Management Strategies Considering Electric Vehicles, Energy Storage Systems, and AI Techniques. *Processes* **2024**, *12*, 270. [CrossRef]
8. Cabana-Jiménez, K.; Candelo-Becerra, J.E.; Sousa Santos, V. Comprehensive Analysis of Microgrids Configurations and Topologies. *Sustain. Sci. Pract. Policy* **2022**, *14*, 1056. [CrossRef]
9. Khodabakhsh, J.; Moschopoulos, G. Simplified Hybrid AC–DC Microgrid with a Novel Interlinking Converter. *IEEE Trans. Ind. Appl.* **2020**, *56*, 5023–5034. [CrossRef]
10. Gong, X.; Dong, F.; Mohamed, M.A.; Abdalla, O.M.; Ali, Z.M. A Secured Energy Management Architecture for Smart Hybrid Microgrids Considering PEM-Fuel Cell and Electric Vehicles. *IEEE Access* **2020**, *8*, 47807–47823. [CrossRef]
11. Espina, E.; Cárdenas-Dobson, R.; Simpson-Porco, J.W.; Sáez, D.; Kazerani, M. A Consensus-Based Secondary Control Strategy for Hybrid AC/DC Microgrids with Experimental Validation. *IEEE Trans. Power Electron.* **2021**, *36*, 5971–5984. [CrossRef]
12. Sahoo, S.; Mishra, S. A Distributed Finite-Time Secondary Average Voltage Regulation and Current Sharing Controller for DC Microgrids. *IEEE Trans. Smart Grid* **2019**, *10*, 282–292. [CrossRef]
13. Yan, H.; Zhou, X.; Zhang, H.; Yang, F.; Wu, Z.G. A Novel Sliding Mode Estimation for Microgrid Control with Communication Time Delays. *IEEE Trans. Smart Grid* **2019**, *10*, 1509–1520. [CrossRef]
14. Shi, S.; Wang, X.; Li, S.; Yang, J. Prescribed-Time Second-Order Sliding Mode Controller Design Subject to Mismatched Term. *IEEE Trans. Circuits Syst. Express Briefs* **2023**, *70*, 1976–1980. [CrossRef]
15. Guo, J. The Load Frequency Control by Adaptive High Order Sliding Mode Control Strategy. *IEEE Access* **2022**, *10*, 25392–25399. [CrossRef]
16. Jiang, H.; Wei, M.; Zhao, Y.; Han, J. Design of Decentralized Adaptive Sliding Mode Controller for the Islanded AC Microgrid with Ring Topology. *Front. Energy Res.* **2021**, *9*, 732997. [CrossRef]

17. Huangfu, Y.; Ma, R.; Miraoui, A. Avoidance High-Frequency Chattering Second-Order Sliding Mode Controller Design: Buck Converter in Wind Power System. *Int. J. Antennas Propag.* **2012**, *2012*, 176830. [CrossRef]
18. Guerrero, J.M.; Chandorkar, M.; Lee, T.L.; Loh, P.C. Advanced Control Architectures for Intelligent Microgrids—Part I: Decentralized and Hierarchical Control. *IEEE Trans. Ind. Electron.* **2013**, *60*, 1254–1262. [CrossRef]
19. Guerrero, J.M.; Loh, P.C.; Lee, T.L.; Chandorkar, M. Advanced Control Architectures for Intelligent Microgrids—Part II: Power Quality, Energy Storage, and AC/DC Microgrids. *IEEE Trans. Ind. Electron.* **2013**, *60*, 1263–1270. [CrossRef]
20. Katiraei, F.; Iravani, R.; Hatziargyriou, N.; Dimeas, A. Microgrids management. *IEEE Power Energ. Mag.* **2008**, *6*, 54–65. [CrossRef]
21. Rakhtala, S.M.; Casavola, A. Real-Time Voltage Control Based on a Cascaded Super Twisting Algorithm Structure for DC–DC Converters. *IEEE Trans. Ind. Electron.* **2022**, *69*, 633–641. [CrossRef]
22. Du, W.; Zhang, J.; Zhang, Y.; Qian, Z. Stability Criterion for Cascaded System with Constant Power Load. *IEEE Trans. Power Electron.* **2013**, *28*, 1843–1851. [CrossRef]
23. Utkin, V. Variable structure systems with sliding modes. *IEEE Trans. Autom. Control.* **1977**, *22*, 212–222. [CrossRef]
24. Songbin, L.; Zhiyuan, F.; Yang, G.; Hai, K.L.; Peng, W. Second-order sliding-mode control of synchronous buck converter based on sub-optimal algorithm. In Proceedings of the 2017 Asian Conference on Energy, Power and Transportation Electrification (ACEPT), Singapore, 24–26 October 2017; pp. 1–6.
25. Kaplan, O.; Bodur, F. Second-order sliding mode controller design of buck converter with constant power load. *Int. J. Control* **2023**, *96*, 1210–1226. [CrossRef]
26. Cucuzzella, M.; Lazzari, R.; Trip, S.; Sandroni, C.; Ferrara, A. Robust voltage regulation of boost converters in DC microgrids. In Proceedings of the 2018 European Control Conference (ECC), Limassol, Cyprus, 12–15 June 2018; pp. 2350–2355.
27. Incremona, G.P.; Cucuzzella, M.; Ferrara, A. Adaptive suboptimal second-order sliding mode control for microgrids. *Int. J. Control* **2016**, *89*, 1849–1867. [CrossRef]
28. Han, Y.; Ma, R.; Cui, J. Adaptive Higher-Order Sliding Mode Control for Islanding and Grid-Connected Operation of a Microgrid. *Energies* **2018**, *11*, 1459. [CrossRef]
29. Baghaee, H.R.; Mirsalim, M.; Gharehpetian, G.B.; Talebi, H.A. Decentralized Sliding Mode Control of WG/PV/FC Microgrids under Unbalanced and Nonlinear Load Conditions for On- and Off-Grid Modes. *IEEE Syst. J.* **2018**, *12*, 3108–3119. [CrossRef]
30. Yoo, H.J.; Nguyen, T.T.; Kim, H.M. Consensus-Based Distributed Coordination Control of Hybrid AC/DC Microgrids. *IEEE Trans. Sustain. Energy* **2020**, *11*, 629–639. [CrossRef]
31. Shen, X.; Liu, J.; Alcaide, A.M.; Yin, Y.; Leon, J.I.; Vazquez, S.; Wu, L.; Franquelo, L.G. Adaptive Second-Order Sliding Mode Control for Grid-Connected NPC Converters with Enhanced Disturbance Rejection. *IEEE Trans. Power Electron.* **2022**, *37*, 206–220. [CrossRef]
32. Lai, J.; Lu, X.; Dong, Z.; Cheng, S. Resilient Distributed Multiagent Control for AC Microgrid Networks Subject to Disturbances. *IEEE Trans. Syst. Man Cybern. Syst.* **2022**, *52*, 43–53. [CrossRef]
33. Xu, Q.; Vafamand, N.; Chen, L.; Dragičević, T.; Xie, L.; Blaabjerg, F. Review on Advanced Control Technologies for Bidirectional DC/DC Converters in DC Microgrids. *IEEE J. Emerg. Sel. Top. Power Electron.* **2021**, *9*, 1205–1221. [CrossRef]
34. Gheisarnejad, M.; Farsizadeh, H.; Khooban, M.H. A Novel Nonlinear Deep Reinforcement Learning Controller for DC–DC Power Buck Converters. *IEEE Trans. Ind. Electron.* **2021**, *68*, 6849–6858. [CrossRef]
35. Hassan, M.A.; Su, C.L.; Pou, J.; Sulligoi, G.; Almakhles, D.; Bosich, D.; Guerrero, J.M. DC Shipboard Microgrids with Constant Power Loads: A Review of Advanced Nonlinear Control Strategies and Stabilization Techniques. *IEEE Trans. Smart Grid* **2022**, *13*, 3422–3438. [CrossRef]
36. Wu, J.; Yang, L.; Lu, Z.; Wang, Q. Robust adaptive composite control of DC–DC boost converter with constant power load in DC microgrid. *Energy Rep.* **2023**, *9*, 855–865. [CrossRef]
37. Yi, S.; Zhai, J. Adaptive second-order fast nonsingular terminal sliding mode control for robotic manipulators. *ISA Trans.* **2019**, *90*, 41–51. [CrossRef] [PubMed]
38. Chen, S.Y.; Chiang, H.H.; Liu, T.S.; Chang, C.H. Precision Motion Control of Permanent Magnet Linear Synchronous Motors Using Adaptive Fuzzy Fractional-Order Sliding-Mode Control. *IEEE/ASME Trans. Mechatron.* **2019**, *24*, 741–752. [CrossRef]
39. Khooban, M.H.; Gheisarnejad, M.; Farsizadeh, H.; Masoudian, A.; Boudjadar, J. A New Intelligent Hybrid Control Approach for DC–DC Converters in Zero-Emission Ferry Ships. *IEEE Trans. Power Electron.* **2020**, *35*, 5832–5841. [CrossRef]
40. Monsalve-Rueda, M.; Candelo-Becerra, J.E.; Hoyos, F.E. Dynamic Behavior of a Sliding-Mode Control Based on a Washout Filter with Constant Impedance and Nonlinear Constant Power Loads. *Appl. Sci.* **2019**, *9*, 4548. [CrossRef]
41. Shtessel, Y.; Edwards, C.; Fridman, L.; Levant, A. *Sliding Mode Control and Observation*; Springer: New York, NY, USA, 2014.
42. Levaggi, L. Sliding modes in Banach spaces. *Differ. Integral Equ.* **2002**, *15*, 167–189. [CrossRef]
43. Triggiani, R. On the stabilizability problem in Banach space. *J. Math. Anal. Appl.* **1975**, *52*, 383–403. [CrossRef]

Disclaimer/Publisher's Note: The statements, opinions and data contained in all publications are solely those of the individual author(s) and contributor(s) and not of MDPI and/or the editor(s). MDPI and/or the editor(s) disclaim responsibility for any injury to people or property resulting from any ideas, methods, instructions or products referred to in the content.